Neuro-Oncology

19(4), 503–513, 2017 | doi:10.1093/neuonc/now230 | Advance Access date 6 January 2017

Glioblastoma on a microfluidic chip: Generating pseudopalisades and enhancing aggressiveness through blood vessel obstruction events

Jose M. Ayuso, Rosa Monge, Alicia Martínez-González, María Virumbrales-Muñoz, Guillermo A. Llamazares, Javier Berganzo, Aurelio Hernández-Laín, Jorge Santolaria, Manuel Doblaré, Christopher Hubert, Jeremy N. Rich, Pilar Sánchez-Gómez, Víctor M. Pérez-García, Ignacio Ochoa*, and Luis J. Fernández*

Group of Applied Mechanics and Bioengineering. Centro Investigación Biomédica en Red. Bioingenieria, Biomateriales y Nanomedicina (CIBER-BBN), Zaragoza, Spain (J.M.A., R.M., M.V.M., G.A.L., M.D., I.O., L.J.F.); Aragón Institute of Engineering Research (I3A), University of Zaragoza, Zaragoza, Spain (J.M.A., R.M., M.V.M., G.A.L., M.D., I.O., L.J.F.); Aragon Institute of Biomedical Research, Instituto de Salud Carlos III, Zaragoza, Spain (J.M.A., R.M., M.V.M., G.A.L., M.D., I.O., L.J.F.); Institute of Applied Mathematics in Science and Engineering, Castilla-La Mancha University, Ciudad-Real, Spain (A.M.G., V.M.P.G.); MEMS/MST Department, Ikerlan S. Coop., Mondragón, Spain (J.B.); Department of Pathology (Neuropathology), Hospital Universitario 12 de Octubre Research Institute, Madrid, Spain (A.H.L.); Department of Design and Manufacturing Engineering, University of Zaragoza,Zaragoza, Spain (J.S.); Department of Stem Cell Biology and Regenerative Medicine, Lerner Research Institute, Cleveland Clinic, Cleveland, Ohio (C.H., J.N.R.); Neuro-oncology Unit. Health Institute Carlos III-UFIEC, Madrid, Spain (P.S.G.)

Corresponding author: Luis José Fernández, PhD, Mailing address: Mariano Esquillor, Zaragoza, Spain, 50018 (luisf@unizar.es).

*These authors coordinated this project equally.

Abstract

Background: Glioblastoma (GBM) is one of the most lethal tumor types. Hypercellular regions, named pseudopalisades, are characteristic in these tumors and have been hypothesized to be waves of migrating glioblastoma cells. These "waves" of cells are thought to be induced by oxygen and nutrient depletion caused by tumor-induced blood vessel occlusion. Although the universal presence of these structures in GBM tumors suggests that they may play an instrumental role in GBM's spread and invasion, the recreation of these structures in vitro has remained challenging.

Methods: Here we present a new microfluidic model of GBM that mimics the dynamics of pseudopalisade formation. To do this, we embedded U-251 MG cells within a collagen hydrogel in a custom-designed microfluidic device. By controlling the medium flow through lateral microchannels, we can mimic and control blood-vessel obstruction events associated with this disease.

Results: Through the use of this new system, we show that nutrient and oxygen starvation triggers a strong migratory process leading to pseudopalisade generation in vitro. These results validate the hypothesis of pseudopalisade formation and show an excellent agreement with a systems-biology model based on a hypoxia-driven phenomenon.

Conclusions: This paper shows the potential of microfluidic devices as advanced artificial systems capable of modeling in vivo nutrient and oxygen gradients during tumor evolution.

Key words

glioblastoma | microfluidics | migration | pseudopalisades | SU-8

Glioblastoma, also known as grade IV astrocytoma, is the most common and lethal malignant primary brain tumor. Patients receiving the standard of care based on local radiotherapy and concomitant chemotherapy have a median survival of 14 months.[1] Despite efforts by the research community, new treatments to tackle this disease are still far from the clinic. GBM tumors are highly infiltrating and rapidly progressing tumors[2] and are characterized by 2 main histopathological conditions: microvascular proliferation and necrotic foci tipically surrounded by areas of high cellularity, known as pseudopalisades[2]

The causes of these densely populated pesudopalisades remain poorly understood. Although the high cellularity was initially thought to be due to rapid proliferation of GBM cells, recent histological studies have shown that proliferation in pseudopalisading areas is significantly lower than in adjacent regions.[3] Additionally, apoptosis in pseudopalisades is substantially larger than in neighboring zones.[4] This evidence suggests that pseudopalisades are due to causes other than simply higher proliferation or survival rates. Recent reports have shown that more than 50% of pseudopalisades in histological slices from GBM patients clearly present a central obstructed blood vessel; microscopic evidence of thrombosis is also observed in more than 90% of samples.[4–6]

GBM cells express several procoagulant factors that may serve to induce thrombosis.[7] Additional evidence shows that cells in pseudopalisades are hypoxic and overexpress HIF-1α.[8] Although this hypoxic microenvironment leads to microvascular hyperplasia, the associated microcirculation is very inefficient due to parenchymal edema and poor maintenance of the blood-brain barrier.[9] As a consequence, the supply of oxygen and nutrients is compromised in the zone surrounding a thrombosis. GBM evolution is a complex process: it has been proposed that one of the driving forces of glioma aggressiveness is nutrient and oxygen starvation.[3,4,10] First, GBM proliferation and secretion of procoagulant signals would causes thrombotic events leading to hypoxia and nutrient depletion. As a consequence, the migration of cells away from a thrombosis and toward nutrients and oxygen-enriched regions could create the characteristic GBM pseudopalisades. Eventually, these migrating cells would reach other blood vessels and eventually cause the collapse of these vessels, restarting the process and creating another expanding wave of tumor cells within the brain. This hypothesis proposes that GBM cells are exposed to cyclic starvation that forces their metabolism to switch between a proliferative or migrating phenotype.

Since we cannot take multiple histologic time points in vivo, it has not been possible to definitively observe thrombosis-induced migration in real time, and the kinetics of any such migration are not understood. This complex process is not reproducible using standard in vitro models because the conventional migration assays are unable to mimic the complex microenvironment described. Recently, microfabrication and microfluidic technologies have arisen, allowing the design and creation of custom, high-performance cell culture systems.[11] In this paper, we describe the design, fabrication, and biological validation of a microfluidic device using SU-8 technology for 3D BM cell cultures under obstructed conditions. In this context, conditions, nutrient starvation leads to a chemotactic process and the formation of a migratory front similar to the pseudopalisades observed in vivo and corresponding to predictive mathematical algorithms. Moreover, our results suggest that the pseudopalisading process stimulates a more aggressive behavior of GBM cells. This novel technique could help us understand the mechanism of pseudopalisade formation and suggest novel therapeutic targets to avoid tumor progression. These microfluidic devices represent an extremely useful platform for evaluating cellular behavior and testing new anticancer agents in a preclinical setting that mimics the complex GBM microenvironment.

Methods

Microfluidic Chip Fabrication

Microfluidic devices were fabricated using SU-8 photolithography combined with an SU-8 to SU-8 bonding process. The fabrication process was inspired by previously reported work describing the fabrication of SU-8 microdevices.[12,13] Briefly, several layers of SU-8 were spun onto the Kapton film, and different soft bake, UV exposure, and post bake steps were performed.[14,15]

Packaging Tool Fabrication

In order to recreate obstructed conditions (Fig. 1A), a regular flow of culture media must be provided to the microdevice through one lateral microchannel, whereas the other is sealed (Fig. 1B). A dedicated package was designed and fabricated to provide proper housing and hermetic connections to the microdevice inlets and outlets, allowing for automated cellular culture. Final microdevice and packaging tool are showed in Fig. 1C.

Cell Culture

C-6 cells were kindly provided by Dr Pešic (University of Belgrade), whereas U-251-MG cells were purchased from ATCC. Both cells were routinely grown in Dulbecco´s modified Eagle´s medium (DMEM) (Lonza BE12-614F) supplemented with 10% v/v fetal bovine serum (Sigma F7524) and penicillin/streptomycin (DE 17-602E) within a TEB-1000 incubator (EBERS Medical Technology). For 3D cultures, all reagents (microdevices included) were placed on ice. Cells were trypsinized and resuspended in a calculated volume of medium (DMEM supplemented with 10 % fetal bovine serum) to reach the desired concentration of cells in the final hydrogel solution. Using a chilled tip, we prepared a mixture of 24.9 µl of collagen type I 4.01 mg/ml (Corning 354236), 0.62 µl of NaOH 1N (Sigma 655104), 10 µl of DMEM 5X (Sigma D5523), 50 µl of cell solution, and 14.5 µl of sterile water. The hydrogel mixture was injected into the device using a micropipette, and then a 5 µl droplet was placed on top of the central inlet to prevent hydrogel leakage and evaporation. Afterwards, the microfluidic device was placed into an incubator (37°C and 5% CO_2) for 15 minutes to allow collagen polymerization. For use as a

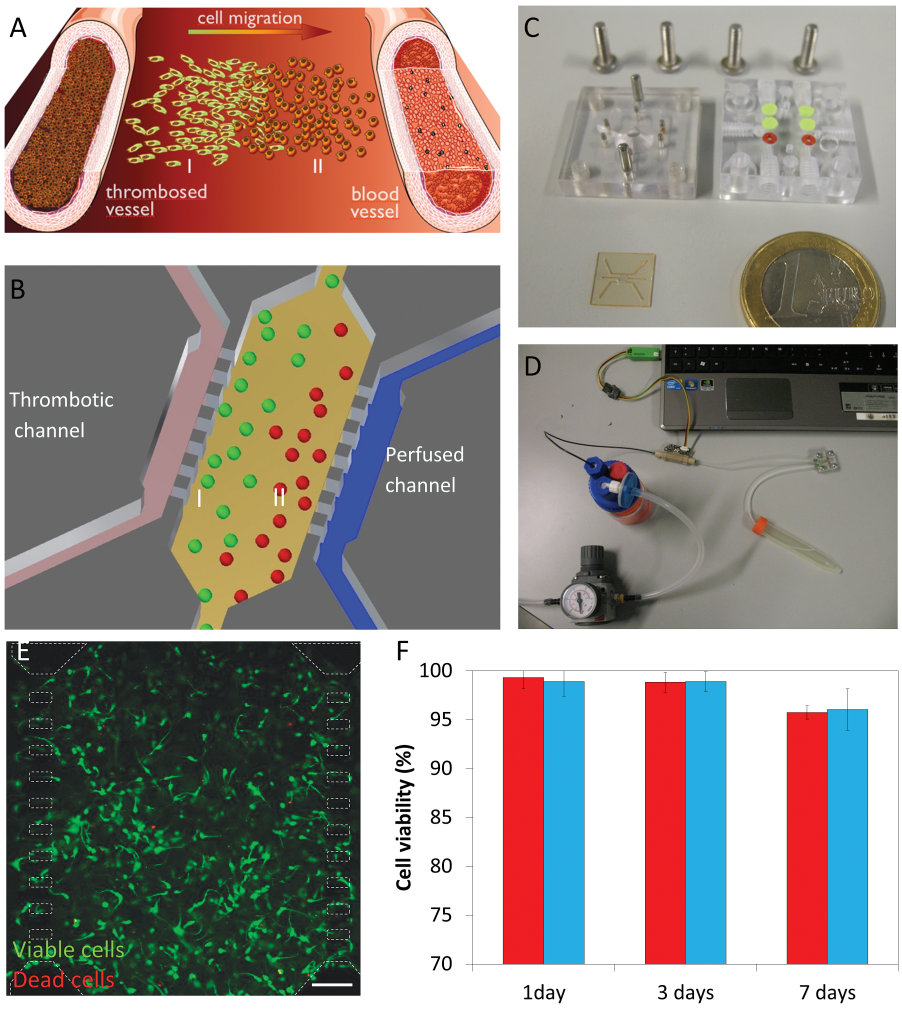

Fig. 1 **Experimental setup.** (A) Scheme of pseudopalisade formation. Under obstructed conditions, nutrient scarcity triggers a migratory response in those cells located in the obstructed blood vessel vicinity (I) towards enriched regions (II). (B) Experimental scheme within the microdevice mimicking the obstructed conditions and the starved (I) and enriched (II) regions. (C) Fabricated microdevice and packaging tool. (D) Microfluidic system. (E) U-251 cell viability within the microdevice after 9 days, live cells (labeled with calcein 1 μg/ml) are shown in green, whereas dead cells are shown in red (labeled with propidium iodide 4 μg/ml). Microdevice posts (50x100 μm) are delimited in white dashed line. Cells were cultured at 4 million cells/ml within a 1.5 mg/ml collagen hydrogel. Viable cells are shown in green, whereas dead cells are shown in red. (F) Comparison of cell viability between hydrogels on Petri dishes (red) and within the microdevice (blue). Cell viability is expressed as the percentage of live cells. Scale bar is 200 μm.

macroscopic control on viability assays, 100 μl of hydrogel mixture were allowed to polymerize on Petri dishes. Medium within microdevices was refreshed once a day. Cell membrane was fluorescently labelled using vibrant DiI (Life Technologies V-22885) following the supplier's instructions.

Cell Viability

Stock solutions of 5 mg/ml calcein (CAM) (LifeTechnologies C1430) and 2 mg/ml propidium iodide (PI) (Sigma P4170) were prepared following supplier instructions.

To test cell viability within microfluidic devices and in Petri dishes, stock solutions of CAM and PI were diluted to 5 and 4 μg/ml, respectively, in phosphate-buffered saline (PBS) (Lonza BE17-516F). Microdevices and Petri controls were washed once with PBS and then filled with CAM/PI. Confocal images were immediately taken using a Nikon Eclipse Ti microscope equipped with a C1 modular confocal microscope system. Images were collected at different focal planes within each microdevice and Petri control.

Long-term Cultures Under Obstructed Conditions

To mimic the obstructed conditions, cells were embedded into a collagen hydrogel injected within the central microchamber of the microdevices. After 24 hours, the microdevices were loaded into the packaging tool, and all inlets were sealed (except for one pair) to enable medium perfusion through only one lateral microchannel

(Fig. 1D). As a control group, other microdevices were left on the Petri dish, and medium was manually refreshed once a day under unrestricted conditions. System evolution was followed, and cell viability and distribution were evaluated at different times. Flow profile was characterized using green-fluorescent 0.2 μm diameter spheres (Life Technologies F8811). Oxygen profile across the microchamber was measured using Image-iT hypoxia reagent (Life Technologies H10498) dissolved in dimethylsulfoxide. Medium supplemented with 10 μM hypoxia reagent was perfused through the system for 24 hours to ensure that the reagent reached the microdevice. Continuous oxygen monitoring throughout the entire experiment was avoided due to the reagent toxicity. Hypoxia-induced fluorescence was detected using a 488 nm laser coupled with a 650nm long-pass detector in the confocal microscope.

Glucose Profile Analysis

The presence of a glucose gradient during experiments was studied using a fluorescent glucose (2-NBDG) (Life Technologies N13195), which is imported by the cells in place of glucose. Since 2-NBDG and conventional glucose compete for the cell glucose transporters, cells were cultured within the microdevices in glucose-free DMEM (Thermo Fisher Scientific 11966-025) supplemented with fetal calf serum, glutamine, and antibiotics. This glucose-free medium was supplemented with 2-NBDG at 200 μM and perfused through one lateral microchannel. Time-lapse images were taken for every 5 minutes for 2 hours to analyze NBDG penetration across the central microchamber. Long-term experiments with NBDG and absence of conventional glucose were not possible since it may affect cell behavior.

Image Analysis

Cell analysis within the central microchamber and Petri controls was performed using automated Fiji software (http://fiji.sc/Fiji). To analyze cell distribution within the central microchamber, only focal planes ranging from 50 μm to 250 μm were used to exclude cells attached directly to the 2D microchamber top and bottom. Selected focal planes were flipped vertically, generating the orthogonal view, which was projected to get the cell distribution across the entire the microchamber length. In order to analyze cell shape, cell perimeter was drawn manually, and ellipse fitted-aspect ratio was calculated as the ratio between the ellipse major and minor axes. Cell directionality was also determined and plotted as a histogram referred to the medium flow direction. At least 100 cells were analyzed in each region.

Immunofluorescence

Samples were fixed for 30 minutes with 4% paraformaldehyde (VWR J61899-AP), permeabilized using 0,1% Triton-X100 (Sigma, T8787) and blocked with 5% bovine serum albumin (Sigma A2058) in PBS. Samples were then incubated overnight with primary antibody (1/50 in 2.5% bovine serum albumin and 0.05% Triton X-100 (Santacruz anti-Ki-67 sc-23900,), and secondary antibody (1/200) was used under the same conditions. DAPI (Sigma D9542-1MG) staining was performed overnight, and step samples were visualized after washing.

Tumor Pathology

The human tissues were procured after obtaining the patients' written consent and with the approval of the ethics committees of Hospital Universitario 12 de Octubre. Hematoxylin and eosin staining was performed on 5 μm thick sections from paraffin-embedded tumors. Pseudopalisades areas were selected, and the nuclear shape in the rear end (close to the necrotic core) or at the front was calculated as previously described. Twenty nuclei were analyzed in each region. Three different samples were analyzed. All methods were carried out in accordance with the approved guidelines.

Mathematical Modeling

This model is based on our previous models[10,16] in which oxygen coming from straight vessels was the driving force that triggered the normoxic and hypoxic phenotypic changes. To these 2 dominant phenotypes, based on the go-or-grow dichotomy,[17] we have incorporated a third phenotype accounting for hypoxic cells that arrive to normoxic areas and switch to a more proliferative phenotype. Also, in addition to the diffusive random motion, we have included a directional transport term driving the cell's motion towards better oxygenated regions for hypoxic cells that was not present in References.[10,16]

The mathematical model consists of a set of partial differential equations modeling the interplay of 3 cellular cancer cell phenotypes, the oxygen distribution, and necrosis:

Major Assumptions of the Mathematical Model:

1. The model is a hybrid between go-or-grow and go-and-grow models.
2. Classical logistic space limited growth for the tumor cell populations.
3. Hypoxic phenotype is more migratory than any other cell phenotype.
4. Oxygen acts as a chemoattractant for hypoxic cells.
5. Malignant cells have the highest proliferation.
6. Oxygen diffusion is homogenous and isotropic in the chamber.
7. Oxygen flows from channels to balance the different oxygen pressures.
8. Malignant cells consume more oxygen than any other cell phenotype.

Statistical Analysis

Data were analyzed using SPSS software, and statistical significance was set at $P < .05$. Results are presented as mean ± standard error. The normal distribution was tested by the Kolmogorov-Smirnov test. For parametric comparison, one-way ANOVA with Bonferroni post hoc

tests was performed. For nonparametric comparisons, a Kruskal-Wallis test was performed followed by the *U* test of Mann-Whitney.

Results

GBM Cells are Viable in 3-Dimensional Microchamber Culture

The fabricated microdevice possesses a central microchamber to locate the cells embedded within a hydrogel,[18–20] mimicking the extracellular matrix and allowing migration in 3 dimensions. On both sides of the microchamber, lateral microchannels are filled with culture medium, allowing nutrient and oxygen diffusion throughout the microchamber and mimicking the function of brain blood vessels.

We first examined microdevice biocompatibility with GBM cells to ensure the material does not affect cell viability. After 7 days in culture, we evaluated U-251 cell viability within microdevices compared with culture dish controls using CAM and PI. Results showed that cell viability within microdevices was very high (>95%); more importantly, it was similar to culture controls at the same time point, thus validating the use of this microdevice for 3D U-251 cell culture (Fig. 1E, F).

Flow Profile

Culture medium supplemented with 1% spheres suspension was injected through the lateral microchannel in obstructed conditions to study the flow profile. Fluorescent time-lapse images demonstrated that the flow profile was not penetrating into the hydrogel under obstructed conditions (supplementary Fig. 1A–C), but it was completely parallel to the central microchamber. When an interstitial flow through the central microchamber was externally imposed, the fluorescent spheres invaded the hydrogel and after 2 minutes a clear invading front was visible (supplementary Fig. 1D–F). Therefore, the fluid flow is not mechanically affecting the hydrogel or the embedded cells under obstructed conditions.

GBM Cells Migrate Under Obstructed Conditions

By controlling medium flow through the lateral microchannels, we can mimic the GBM-associated thrombotic pathophysiological conditions. Under unrestricted conditions, cell distribution within the microchamber was constant throughout the experiment (9 days of culture, Fig. 2A–C). Under obstructed conditions, cell viability continued to be very high (>95%), and we also observed a strong migratory process. After 3 days of thrombotic conditions, cell migration was barely apparent, and only small cell aggregates near the perfused microchannel were visible (Fig. 2D). After 6 days, migration evolved to the formation of a well-defined front, resembling the in-vivo observed pseudopalisades (Fig. 2E). Finally, after 9 days, this front moved closer to and invaded the perfused microchannel (Fig. 2F). In order to perform a more quantitative and precise analysis, we analyzed the fluorescence intensity across the microchamber. This analysis of cell distribution confirmed that there was no change during the time course under unrestricted conditions (Fig. 2G-I). On the other hand, after 3 days under obstructed conditions this distribution showed a moderate increase near the perfused lateral microchannel compared with the unrestricted conditions, showing an emerging migratory response (Fig. 2H). After 6 days, this response increased to a well-defined peak, indicating cells concentrating in this region, creating the characteristic pseudopalisade front, and abandoning the occluded rear region. After 9 days, the intensity of the pseudopalisade front reached a maximum and was displaced as cells reached the perfused lateral microchannel. This is the first experimental evidence showing the creation of a pseudopalisade front by a migratory wave of GBM cells moving from obstructed to perfused conditions. In order to expand this study using another GBM cell line, C-6 cells were cultured in the microdevice under similar conditions. After 3 days under obstructed conditions, C-6 cells showed an invasion process towards the perfused lateral microchannel (supplementary Fig. 2). Interestingly, C-6 cells exhibited a faster invasion than U-251 MG. Furthermore, a population of dead C-6 cells appeared concentrated nearby the obstructed lateral microchannel. Thereby, C-6 cells seemed to have a faster metabolism compared with U-251 MG, which led to an accelerated invasion. Longer invasion times using C-6 cells were not analyzed due to a significant hydrogel contraction caused by these cells.

Cell Morphology Analysis During Pseudopalisade Formation

Our results suggested that pseudopalisading structures can be created by a migratory response led by cells located at the rear of the migratory front near the nonperfused microchannel. We next investigated the morphologic changes in GBM cells during the formation of pseudopalisades. Cells under unrestricted conditions appeared identical on either side of the microchamber, which was expected after 4 days of culture (Fig. 3A). Conversely, cell morphology clearly shifted in the cell population closest to the obstructed channel 5 days after the induction of obstructed conditions (Fig. 3B). In the rear, cells greatly increased in aspect ratio (5.3 ± 2.3) and became highly elongated with very large protrusions, whereas cells in the front were mainly rounded with aspect ratio close to one (1.2 ± 0.2) ($P < .001$) (Fig. 3C). We analyzed cell directionality near the obstructed channel and found a bias towards the medium flow (Fig. 3D). Cell directionality in those regions with lower aspect ratio (1–1.5) was not analyzed since this parameter is irrelevant in rounded cells. Interestingly, we observed the same cellular pattern in the pseudopalisades detected in human GBM samples, with a significant change in the nucleus-aspect ratio (2.1 ± 0.5) in the rear end (close to the necrotic core) compared with the front (1.3 ± 0.2) (Fig. 3E and F).

Characterization of Pseudopalisade Formation

A recent hypothesis about GBM suggests that when migrating cells forming the pseudopalisade reach a new, nutrient-rich microenvironment (ie, in the vicinity of a perfused blood vessel), their metabolism reverts to a more

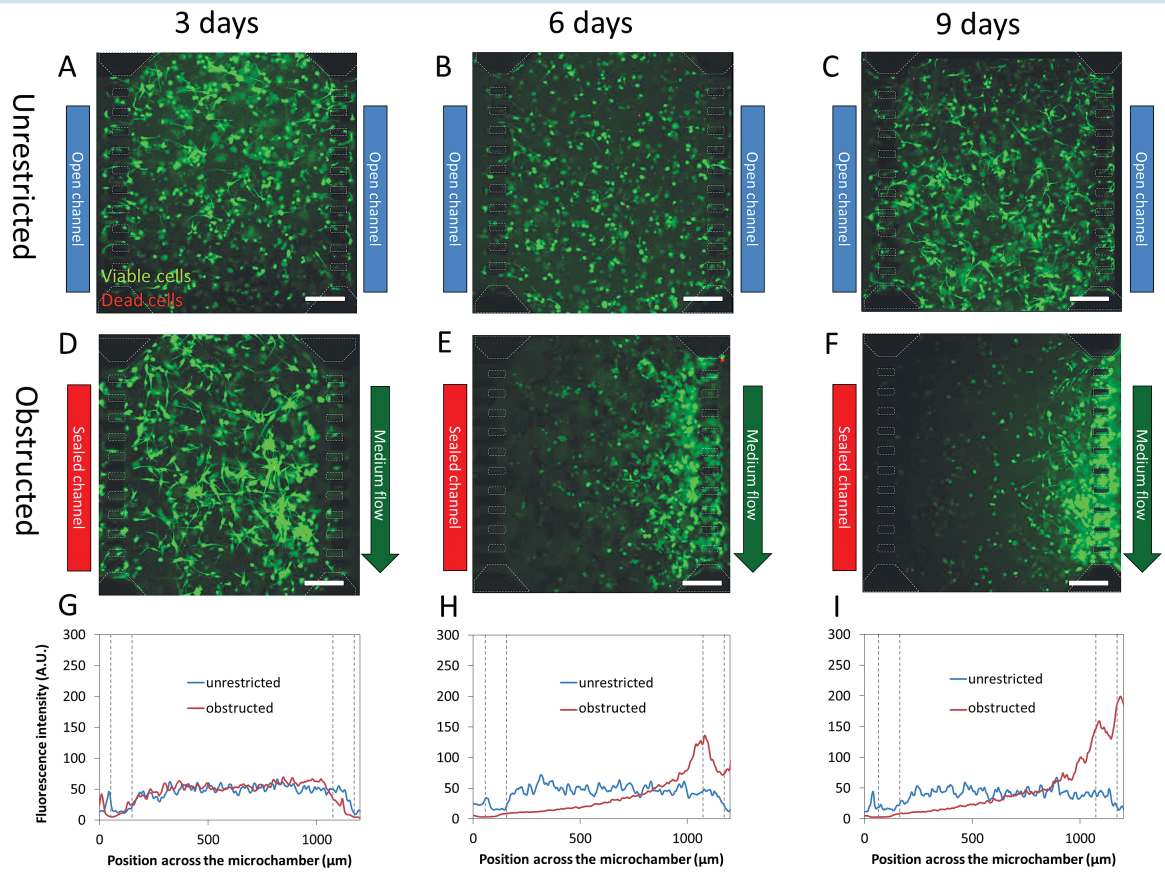

Fig. 2 Pseudopalisade formation under obstructed conditions. U-251 at 4 million cells/ml in collagen hydrogel at 1.5 mg/ml was cultured within microdevices. Under unrestricted conditions, medium was refreshed once a day, and cell viability was evaluated at 3 (A), 6 (B), and 9 (C) days using calcein (green) and propidium iodide (red). To mimic obstructed conditions, medium flow was enabled only through right microchannel, and cell viability was assessed at 3 (D), 6 (E), and 9 (F) days. Microdevice posts (50x100 µm) are delimited in white dashed line. Graphs show the fluorescence intensity across the microchamber orthogonal view at 3 (G), 6 (H), and 9 days (I) in obstructed as unrestricted conditions. Post position in the graphs is delimited by gray dashed lines. Scale bar is 200 µm.

proliferative and less migratory state. To test this hypothesis within our system, we analyzed cell proliferation under the different stages of pseudopalisade formation by Ki-67 immunofluorescence. After 5 days under obstructed conditions, we observed no Ki-67 positive cells (Fig. 4A). On the other hand, when the pseudopalisade was completely formed after 9 days under obstructed conditions, positive cells were observed (Fig. 4B). More interestingly, those proliferative cells appeared only in the vicinities of the perfused microchannel (where nutrient concentrations are expected to be highest). Under unrestricted conditions, we did not observe positive cells after either 5 or 9 days (Fig. 4C and D). The central microchamber was vertically divided into 3 regions, and the number of proliferating cells was determined in each (Fig. 4E). The analysis demonstrated that most of the proliferating cells were located on the region closest to the perfused lateral microchannel; only a small proportion appeared in the central region, and no proliferating cells were observed in the further region.

To determine if a glucose gradient was generated during long-term experiments, we analyzed the diffusion profile of the fluorescent glucose analog 2-deoxy-2-[(7-nitro-2,1,3-benzoxadiazol-4-yl)amino]-D-glucose (NBDG) across the microchamber in the absence or presence of cells (supplementary Fig. 3) during 2 hours post-NBDG injection. We found little difference in cellular glucose uptake across the microchamber, and cells were able to uptake the NBDG. The NBDG diffusion profile without cells (green line) was very similar to the NBDG profile in the presence of cells (red line). (Note: the dark areas observed in the assay-containing cells are due to light scattering from cells out of the focal plane [supplementary Fig. 4]). After removing the NBDG, the cells remained labeled in green, showing their ability to incorporate the glucose analog (supplementary Fig. 5). This indicates that during long-term experiments, GBM cells are not exposed to a significant glucose gradient and further suggests that pseudopalisading formation is driven by factors other than glucose scarcity.

We next investigated the oxygen profile across the microchamber during experiments using Image-it hypoxia reagent, which becomes fluorescent as oxygen tension decreases. Two different sets of experiments were performed, and both were carried out for 5 days. Under

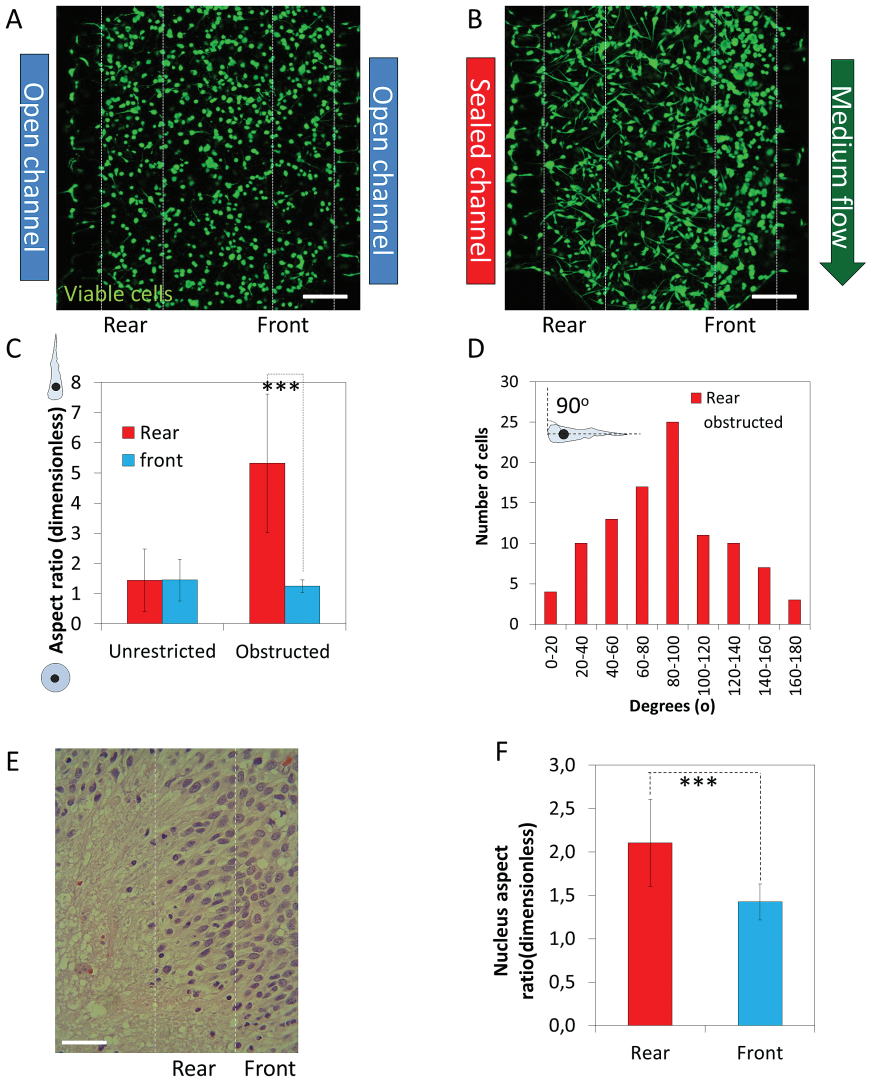

Fig. 3 Cell shape during pseudopalisade formation. Confocal images of the microchamber were taken after 5 days in culture under unrestricted (A) or obstructed conditions (B). (C) Cell shape at the pseudopalisade rear and front was analyzed and compared with the same region under unrestricted conditions; *** denotes a statistical difference (*P* value $1.4x10^{-32}$). (D) Directionality at the pseudopalisade rear under obstructed conditions. (E) Hematoxylin and eosin staining of a paraffin-embedded GBM sample. (F) Nucleus aspect ratio in the pseudopalisade rear and front in patient samples; *** denotes a statistical difference (*P* value $3.7x10^{-8}$). Scale bar is 200 μm.

unrestricted conditions, medium was pipetted only once a day through both lateral microchannels. Since both lateral microchannels remained open, the oxygen consumption was symmetric; thereby, a homogeneous hypoxia along the microchamber was generated (Fig. 5A and supplementary Fig. 6A).

On the other hand, under obstructed conditions the medium flow through the right lateral microchannel guaranteed that oxygen and nutrients in the perfused lateral microchannel were continuously refreshed, whereas the opposed lateral microchannel remained blocked. Thereby, those cells located near the perfused microchannel showed very low hypoxia-induced fluorescence intensity, suggesting a normoxic microenvironment, whereas those cells located near the blocked microchannel showed the highest hypoxia-induced fluorescence intensity (Fig. 5B, C and supplementary Fig. 5B).

These results showed that under unrestricted conditions, when a homogenous and constant hypoxia was present across the microchamber, no directional migration was observed. Interestingly, when a hypoxia gradient was generated, directional migration was observed.

Correlation of Computer Simulations with Experimental Data

Since the migratory response of the GBM cells is nonlinear and not entirely intuitive, we investigated the correlation of our experimental data with simulated computer models. Under unrestricted conditions, the number of cells and their distribution along the chamber varied only slightly due to the very slow proliferation rates we observed (Fig. 6A). In our computer simulations, all cells have a normoxic phenotype

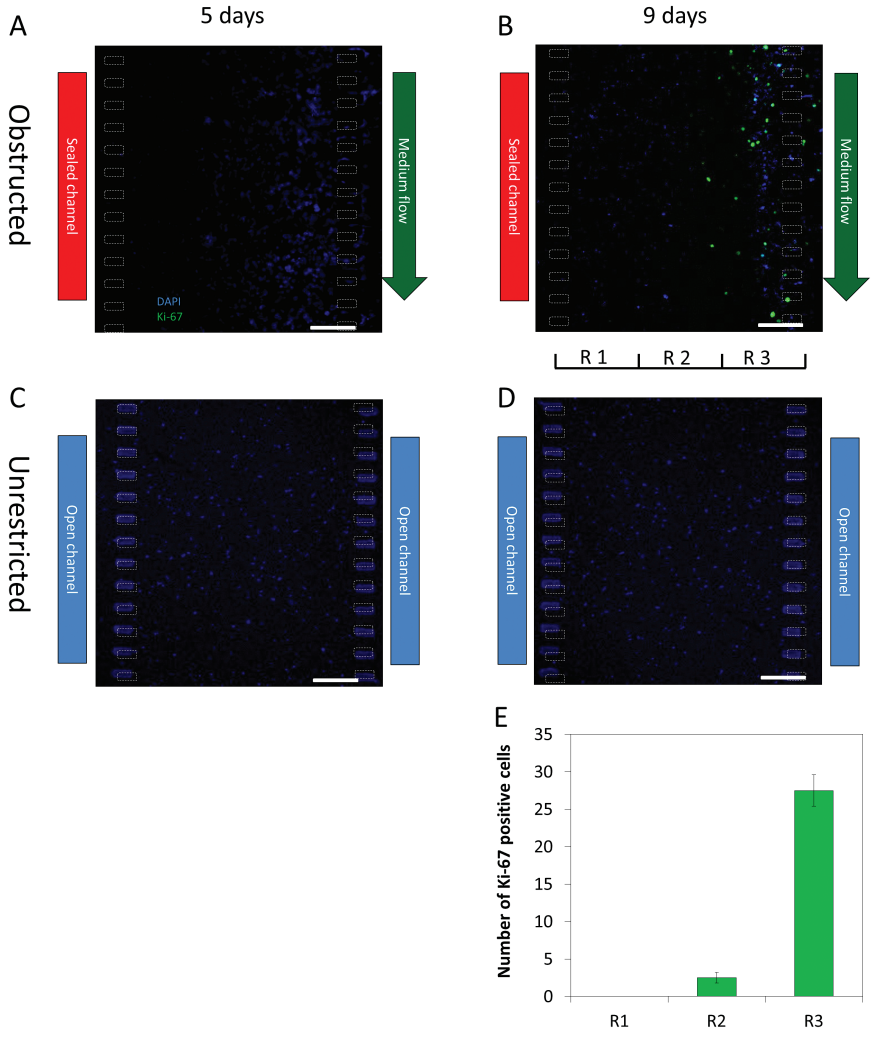

Fig. 4 **Proliferation during pseudopalisade formation.** Ki-67 immunofluorescence was performed within the microdevices during the different steps of the pseudopalisade formation. (A–B) Under obstructed conditions, ki-67 positive cells were observed only after 9 days, when the pseudopalisade was completely formed. (C–D) Under unrestricted conditions, no positive cells were observed at 5 or 9 days. (ED) Quantitative analysis of Ki-67 positive cells in the three regions deffined in "B". Scale bar is 200 μm.

after 9 days. When the nutrient flow along the left channel was disrupted, cellularity remained spatially homogeneous for 3 days while the nutrient level became exhausted, after which cells slowly changed their phenotypes. However, our numerical simulations revealed the formation of a pseudopalisade structure moving towards the active channel after 6 days and a dramatic increase in cell density around the flow channel at day 9 (Fig. 6B), which concurs strongly with our experiments. Fig. 8C shows the mathematical model scheme used in the computational simulations. We have performed extensive parameter value scans, and we are forced to conclude that the dynamic behavior observed in our experimental model cannot be reproduced within the framework of the previously published 2-phenotype computational model.[10,16] This model assumes that tumor cells revert to their original normoxic phenotypes when reaching areas of higher oxygenation. Instead, the incorporation of a third, highly proliferative phenotype after the wave of migration is essential to reproduce the evolution of our observed cell density profiles during pseudopalisade generation. Our analysis suggests the existence of a highly proliferative GBM cell state triggered by transient waves of metabolic deprivation and migration (Fig. 6C).

Discussion

Nutrient and oxygen depletion, due to blood vessel obstruction events, plays an important role in the accelerated spread of GBM cells across the brain. In this work, we provide a robust and novel methodology to mimic the GBM-associated blood vessel obstruction in vitro. Using our developed microdevice, we were able to culture GBM cells under induced obstructed conditions, and for the first time we can demonstrate the formation of a pseudopalisade-like front through several sequential steps. In an initial stage, during the first days under obstructed conditions, there is little morphologic change in the GBM cells as remaining oxygen and nutrients are consumed. In a second stage, nutrient starvation leads to

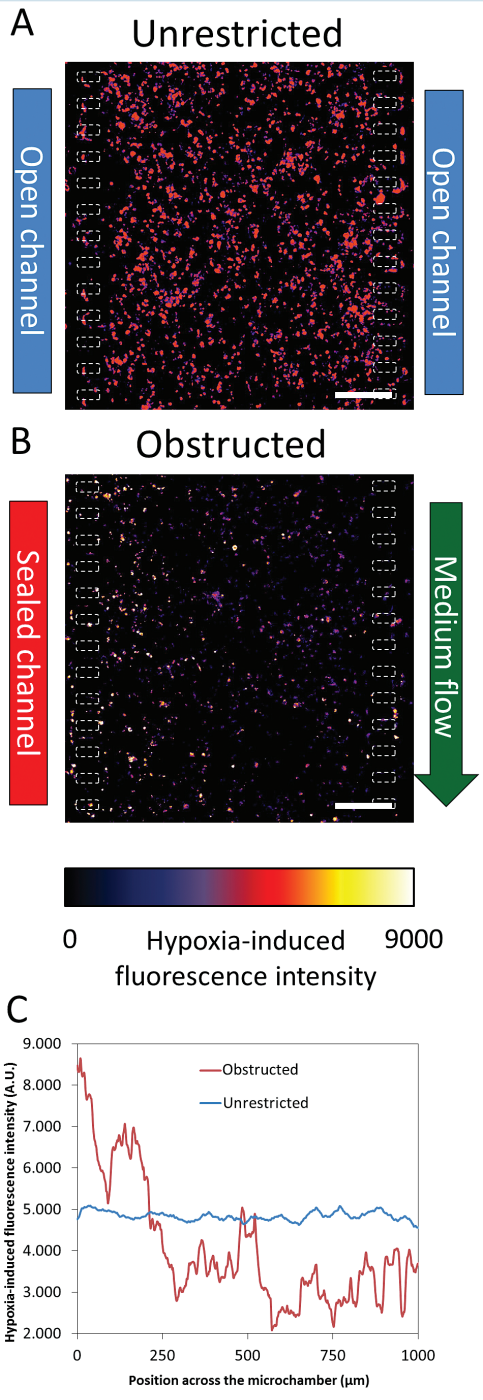

Fig. 5 **Oxygen profile.** Oxygen profile was detected after 5 days in culture using Image-it Hypoxia reagent. Images are shown as heat-map hypoxia-induced fluorescence intensity. Hypoxia-induced fluorescence intensity across the microchamber revealed that oxygen concentration was constant under unrestricted conditions (A), whereas an oxygen gradient was established under obstructed conditions (B). The graph shows the hypoxia-induced fluorescence intensity profile across the microchamber (C). Scale bar is 200 μm.

an intense migratory response in those cells located in the starved region (ie, the pseudopalisade rear). This migratory response creates the observed pseudopalisading structures after 6 days in culture. Finally, in a third stage, cells of this pseudopalisade front reach the nutrient source (invading the perfused lateral microchannel) and undergo rapid proliferation. This behavior models GBM pseudopalisade progression observed in patients and enables the study of this phenomenon in vitro. The pseudopalisading hypothesis has been suggested to explain the poor improvement on mean survival time achieved by conventional antitumorigenic treatments.[21] Accordingly, the approved chemotherapy treatment for GBM, based on concomitant doses of the alkylating chemotherapy agent temozolomide combined with radiotherapy, only improves mean survival time by a few months compared with radiotherapy alone.[1,21] Since most such treatments are focused on killing proliferative cells, they do not target those nonproliferative migratory cells of pseudopalisades. Unfortunately, once these cells reach nutrient-rich regions, they can once again become proliferative.

Many recent reports show that cell migration plays a critical role on GBM invasion and spread, correlating with patient prognosis.[22–24] In this context, new drugs are being developed to block GBM cell migration.[25] Thus, different animal and in vitro studies show that treatment with specific migration inhibitors can achieve a significantly mean survival time improvement.[26,27] It has been shown that GBM cells invade by a mesenchymal migration mode[28–30] based on integrins and matrix-degrading enzymes such as membrane type matrix metalloproteinase-1 (MT-MMP-1) and MMP-2.[31,32] These proteins are normally overexpressed in GBM.[33] More interestingly, recent reports have shown that hypoxia, through HIF-1α, induces an epithelial-mesenchymal transition in GBM cell lines that enhances cell invasiveness.[34] In our model, cells showed this expected mesenchymal-like GBM migration mode, including the characteristic emission of invadopodia and the very large aspect ratio.[35] Our directionality distribution showed that rear cells were preferentially orientated towards the perfused lateral microchannel (the oxygen and nutrient source), forming an angle of 90° with medium flow and aligning in the direction of travel during pseudopalisade formation.

Our oxygen profile measurements reveal that cell metabolism creates an oxygen gradient across the microchamber under obstructed conditions that resembles the hypoxic areas observed in in-vivo pseudopalisades. Our mathematical model suggests the development of a more malignant phenotype after these cycles of hypoxia, migration, and reoxygenation. This phenotype is highly proliferative and oxygen dependent. Our mathematical simulations support the hypothesis of pseudopalisade formation after a vessel-occlusion event and correlate very well with microfluidic device experiments in which we saw an increase in the cell proliferation when the cells where exposed to obstructed conditions. Our results suggest that when these invading and hypoxic GBM cells reach a better oxygenated region, they start to proliferate more aggressively. Therefore, microscopic hypoxic events can act as a driving force in GBM invasion. Therefore, this mathematical model is able to recapitulate the pseudopalisade formation as a hypoxia-driven phenomenon, convincingly reproducing the observed results within the microdevice and the observed pseudopalisades in vivo.

Our interdisciplinary approach now allows direct observation of GBM invasion and pseudopalisade formation under controlled conditions. Furthermore, the mathematical modeling suggests a sequence of cell states that include alternating phases of hypoxia, invasiveness, and proliferation.

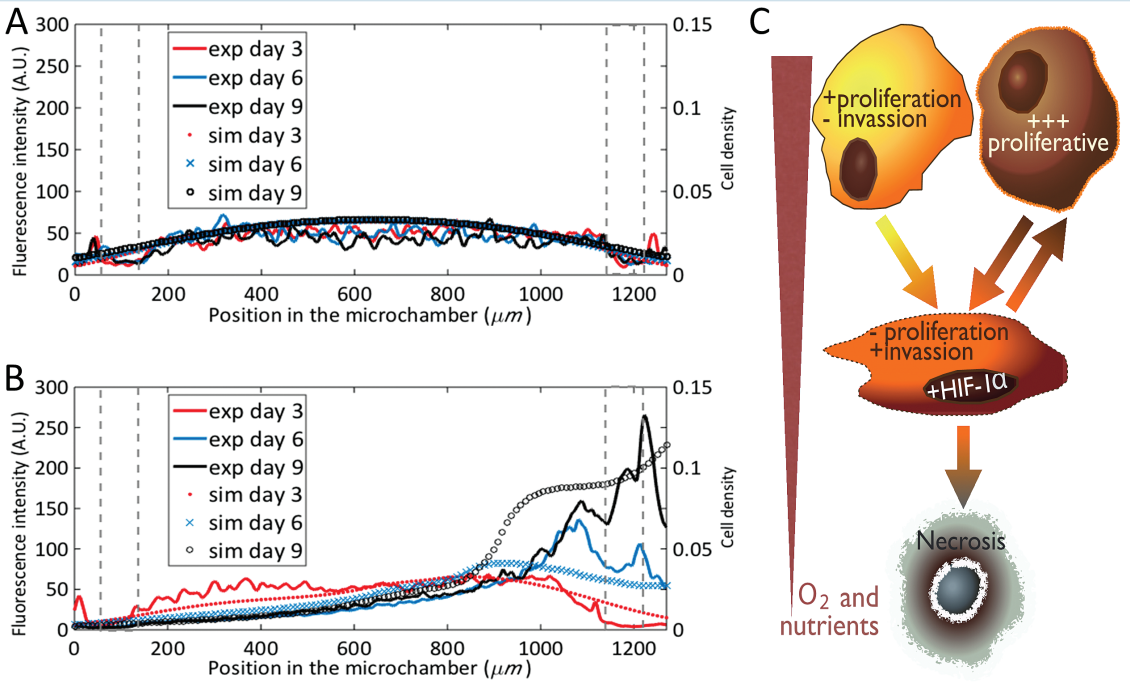

Fig. 6 **Computer simulations versus experimental data of the cell evolution profiles.** Simulations of tumor cell density evolution and experimental data of fluorescence intensity within the chamber under unrestricted conditions (A) and under obstructed conditions (B). Left Y axis denotes fluorescence intensity from experiments at days 3, 6, and 9, curves red, blue, and black, respectively. Right Y axis denotes cell density from simulations at days 3, 6, and 9, red spots, blue cross, and black circles, respectively. Post position in the graphs is delimited by gray dashed line. (C) Graphical depiction of the mathematical model scheme based on previous models [10, 13] including 3 cancer cell phenotypes, the oxygenation and the necrosis (C).

These methodologies enable us to see processes once found only in vivo and shed light on the states and life cycle of GBM, which could enable more biologically accurate drug screening methods focused on GBM invasion.

Supplementary Material

Supplementary material is available online at *Neuro-Oncology* (http://neuro-oncology.oxfordjournals.org/).

Funding

Projects (DPI2011-28262c04-01), (DPI2015-65401-C3-1-R), (BIO2016-79092-R), (MTM2015-71200-R), (BES-2012-059940)"; and the "Junta de Comunidades de Castilla-La Mancha/FEDER" (PEII-2014-031-P). "Ministerio de Economía y Competitividad, Fondo de Investigación Sanitaria" (PI12/00775 to P.S.G., PI13/01258 to A.H.L); "Ministerio de Economía y Competitividad, Red Temática de Investigación Cooperativa en Cancer" (RD12/0036/0027 to P.S.G. and A.H.L.) and by The National Institutes of Health (CA189647 to C.G.H.; CA154130, CA171652, CA169117, NS087913, and NS089272 to J.N.R); Research Program Committees of Cleveland Clinic (J.N.R), and James S. McDonnell Foundation (J.N.R). James S. Mc. Donnell Foundation (USA) 21st Century Science Initiative in Mathematical and Complex Systems approaches for Brain Cancer (Special Initiative Collaborative Planning Grant 220020420 and Collaborative award 220020450. Morgridge Insitute for Research.

Acknowledgments

The authors thank Dr Mario Durán for all the scientific support and useful discussions. Thanks to José Luis Calavia for his technical support related with the microfluidic system connections and monitoring. Thanks to Dr Pesic for her advice about the C-6 cells.

Conflict of interest statement. All the authors declare no competing interests.

References

1. Oike T, Suzuki Y, Sugawara K, et al. Radiotherapy plus concomitant adjuvant temozolomide for glioblastoma: Japanese mono-institutional results. *PLoS One*. 2013;8(11):e78943.
2. Brat DJ, Kaur B, Van Meir EG. Genetic modulation of hypoxia induced gene expression and angiogenesis: relevance to brain tumors. *Front Biosci*. 2003;8:100–116.
3. Rong Y, Durden DL, Van Meir EG, Brat DJ. 'Pseudopalisading' necrosis in glioblastoma: a familiar morphologic feature that links vascular pathology, hypoxia, and angiogenesis. *J Neuropathol Exp Neurol*. 2006;65(6):529–539.

4. Brat DJ, Castellano-Sanchez AA, Hunter SB, et al. Pseudopalisades in glioblastoma are hypoxic, express extracellular matrix proteases, and are formed by an actively migrating cell population. *Cancer Res*. 2004;64(3):920–927.
5. Wippold FJ 2nd, Lämmle M, Anatelli F, Lennerz J, Perry A. Neuropathology for the neuroradiologist: palisades and pseudopalisades. *AJNR Am J Neuroradiol*. 2006;27(10):2037–2041.
6. Rong Y, Post DE, Pieper RO, Durden DL, Van Meir EG, Brat DJ. PTEN and hypoxia regulate tissue factor expression and plasma coagulation by glioblastoma. *Cancer Res*. 2005;65(4):1406–1413.
7. Brat DJ, Van Meir EG. Vaso-occlusive and prothrombotic mechanisms associated with tumor hypoxia, necrosis, and accelerated growth in glioblastoma. *Lab Invest*. 2004;84(4):397–405.
8. Jensen RL. Brain tumor hypoxia: tumorigenesis, angiogenesis, imaging, pseudoprogression, and as a therapeutic target. *J Neurooncol*. 2009;92(3):317–335.
9. Jain RK, di Tomaso E, Duda DG, Loeffler JS, Sorensen AG, Batchelor TT. Angiogenesis in brain tumours. *Nat Rev Neurosci*. 2007;8(8):610–622.
10. Martínez-González A, Calvo GF, Pérez Romasanta LA, Pérez-García VM. Hypoxic cell waves around necrotic cores in glioblastoma: a biomathematical model and its therapeutic implications. *Bull Math Biol*. 2012;74(12):2875–2896.
11. Bhatia SN, Ingber DE. Microfluidic organs-on-chips. *Nat Biotechnol*. 2014;32(8):760–772.
12. Blanco FJ, Agirregabiria M, Garcia J, et al. Novel three-dimensional embedded SU-8 microchannels fabricated using a low temperature full wafer adhesive bonding. *J Micromech Microeng*. 2004;14(7):10.
13. Ayuso JM, Monge R, Llamazares G, et al. SU-8 based microdevices to study self-induced chemotaxis in 3D microenvironments. *Front Mater*. 2015;2:37.
14. Altuna A, Bellistri E, Cid E, et al. SU-8 based microprobes for simultaneous neural depth recording and drug delivery in the brain. *Lab Chip*. 2013;13(7):1422–1430.
15. Altuna A, Menendez de la Prida L, Bellistri E, et al. SU-8 based microprobes with integrated planar electrodes for enhanced neural depth recording. *Biosens Bioelectron*. 2012;37(1):1–5.
16. Martínez-González A, Durán-Prado M, Calvo GF, Alcaín FJ, Pérez-Romasanta LA, Pérez-García VM. Combined therapies of antithrombotics and antioxidants delay in silico brain tumour progression. *Math Med Biol*. 2015;32(3):239–262.
17. Hatzikirou H, Basanta D, Simon M, Schaller K, Deutsch A. 'Go or grow': the key to the emergence of invasion in tumour progression? *Math Med Biol*. 2012;29(1):49–65.
18. Jeong GS, Han S, Shin Y, et al. Sprouting angiogenesis under a chemical gradient regulated by interactions with an endothelial monolayer in a microfluidic platform. *Anal Chem*. 2011;83(22):8454–8459.
19. Kim C, Kasuya J, Jeon J, Chung S, Kamm RD. A quantitative microfluidic angiogenesis screen for studying anti-angiogenic therapeutic drugs. *Lab Chip*. 2015;15(1):301–310.
20. Kothapalli CR, van Veen E, de Valence S, et al. A high-throughput microfluidic assay to study neurite response to growth factor gradients. *Lab Chip*. 2011;11(3):497–507.
21. Peponi E, Tourkantonis I, Tasiou I, Pavlidis N, Pentheroudakis G, Tsekeris P. Prognostic factors in glioblastoma patients managed with radiotherapy combined with temozolomide. *J BUON*. 2014;19(3):718–723.
22. Vehlow A, Cordes N. Invasion as target for therapy of glioblastoma multiforme. *Biochim Biophys Acta*. 2013;1836(2):236–244.
23. Møller HG, Rasmussen AP, Andersen HH, Johnsen KB, Henriksen M, Duroux M. A systematic review of microRNA in glioblastoma multiforme: micro-modulators in the mesenchymal mode of migration and invasion. *Mol Neurobiol*. 2013;47(1):131–144.
24. Lefranc F, Brotchi J, Kiss R. Possible future issues in the treatment of glioblastomas: special emphasis on cell migration and the resistance of migrating glioblastoma cells to apoptosis. *J Clin Oncol*. 2005;23(10):2411–2422.
25. Scaringi C, Minniti G, Caporello P, Enrici RM. Integrin inhibitor cilengitide for the treatment of glioblastoma: a brief overview of current clinical results. *Anticancer Res*. 2012;32(10):4213–4223.
26. Munson JM, Fried L, Rowson SA, et al. Anti-invasive adjuvant therapy with imipramine blue enhances chemotherapeutic efficacy against glioma. *Sci Transl Med*. 2012;4(127):127ra136.
27. Zhang L, Wang H, Zhu J, Ding K, Xu J. FTY720 reduces migration and invasion of human glioblastoma cell lines via inhibiting the PI3K/AKT/mTOR/p70S6K signaling pathway. *Tumour Biol*. 2014;35(11):10707–10714.
28. Myung JK, Choi SA, Kim SK, Wang KC, Park SH. Snail plays an oncogenic role in glioblastoma by promoting epithelial mesenchymal transition. *Int J Clin Exp Pathol*. 2014;7(5):1977–1987.
29. Piao Y, Liang J, Holmes L, Henry V, Sulman E, de Groot JF. Acquired resistance to anti-VEGF therapy in glioblastoma is associated with a mesenchymal transition. *Clin Cancer Res*. 2013;19(16):4392–4403.
30. Caspani EM, Echevarria D, Rottner K, Small JV. Live imaging of glioblastoma cells in brain tissue shows requirement of actin bundles for migration. *Neuron Glia Biol*. 2006;2(2):105–114.
31. Hotary K, Allen E, Punturieri A, Yana I, Weiss SJ. Regulation of cell invasion and morphogenesis in a three-dimensional type I collagen matrix by membrane-type matrix metalloproteinases 1, 2, and 3. *J Cell Biol*. 2000;149(6):1309–1323.
32. Friedl P. Prespecification and plasticity: shifting mechanisms of cell migration. *Curr Opin Cell Biol*. 2004;16(1):14–23.
33. Yamamoto M, Ueno Y, Hayashi S, Fukushima T. The role of proteolysis in tumor invasiveness in glioblastoma and metastatic brain tumors. *Anticancer Res*. 2002;22(6C):4265–4268.
34. Joseph JV, Conroy S, Pavlov K, et al. Hypoxia enhances migration and invasion in glioblastoma by promoting a mesenchymal shift mediated by the HIF1α-ZEB1 axis. *Cancer Lett*. 2015;359(1):107–116.
35. Yilmaz M, Christofori G, Lehembre F. Distinct mechanisms of tumor invasion and metastasis. *Trends Mol Med*. 2007;13(12):535–541.